High accuracy polarization measurements using binary polarization rotators

X. Steve Yao[1, 2]*, Xiaojun Chen[2], and Tiegen Liu[1]

[1]*Optical Polarization Research Center and Key Laboratory of Opto-electronics Information and technical Science of China Ministry of Education, College of Precision Instrument and Opto-electronics engineering,Tianjin University, Tianjin, 300072, China*

[2]*General Photonics Corporation, 5228 Edison Av., Chino, CA 91710, USA*

syao@generalphotonics.com

Abstract: We report a novel system for the accurate measurement of all polarization related parameters, including polarization mode dispersion and polarization dependent loss, using binary magneto-optic polarization rotators. By taking advantage of the binary nature of the rotators, we achieved unprecedented DGD, SOPMD, and PDL accuracies of 2.6 fs, 1.39ps^2, and 0.06 dB respectively; repeatabilities of 0.022 fs, 0.28 ps^2, and 0.034dB respectively; and resolutions of 1 fs, 0.005 ps^2 and 0.01dB respectively, from 1480 to 1620 nm.

OCIS codes: (120.5410) Polarimetry; (080.2730) Matrix methods in paraxial optics; (060.2300) Fiber measurements; (260.5430) Polarization; Polarization mode dispersion; Polarization dependent loss.

References and links

1. X. S. Yao, "Controlling polarization related impairments," Lightwave Magazine, October 31, 2000.
2. H. Kogelnik, R. Jopson, and L. Nelson, "Polarization-Mode Dispersion," in *Optical Fiber telecommunications, Vol. IV-B, Systems and Impairments*, I. P. Kaminow and L. Tingye ed., (Elsevier Science (USA)
3. E. Lichtman, "Limitations imposed by polarization-dependent gain and loss on all-optical ultralong communication systems," J. Lightwave Technol. **13**(5), 906–913 (1995).
4. X. S. Yao, L.-S. Yan, B. Zhang, A. E. Willner, and J. Jiang, "All-optic scheme for automatic polarization division demultiplexing," Opt. Express **15**(12), 7407–7414 (2007).
5. E. Ip, A. P. Lau, D. J. Barros, J. M. Kahn, "Coherent detection in optical fiber systems," Opt. Express **16**(2), 753–791 (2008).
6. H. Sun, K. T. Wu, and K. Roberts, "Real-time measurements of a 40 Gb/s coherent system," Opt. Express **16**(2), 873–879 (2008).
7. R. A. Chipman, and Ch. Polarimetry, 22 in Handbook of Optics, vol. II, 2nd Ed. M. Bass ed., McGraw-Hill, New York, 1995.
8. D. H. Goldstein, "Mueller matrix dual-rotating retarder polarimeter," Appl. Opt. **31**(31), 6676–6683 (1992).
9. P. A. Williams, "Rotating-wave-plate stokes polarimeter for differential group delay measurements of polarization-mode dispersion," Appl. Opt. **38**(31), 6508–6515 (1999).
10. E. Dijkstra, H. Meekes, and M. Kremers, "The high-accuracy universal polarimeter," J. Phys. **24**(10), 1861–1868 (1991).
11. P. A. Williams, A. H. Rose, and C. M. Wang, "Rotating-polarizer polarimeter for accurate retardance measurement," Appl. Opt. **36**(25), 6466–6472 (1997).
12. A. De Martino, Y. K. Kim, E. Garcia-Caurel, B. Laude, and B. Drévillon, "Optimized Mueller polarimeter with liquid crystals," Opt. Lett. **28**(8), 616–618 (2003).
13. B. Wang, J. List, and R. Rockwell, "Stokes polarimeter using two photoelastic modulators," in Polarization Measurement, Analysis, and Applications V, D. H. Goldstein and D. B. Chenault, eds., Proc. SPIE 4819, 1–8 (2002).
14. R. M. A. Azzam, "Arrangement of four photodetectors for measuring the state of polarization of light," Opt. Lett. **10**(7), 309–311 (1985).
15. R. M. Craig, S. L. Gilbert, and P. D. Hale, "High-resolution, nonmechanical approach to polarization-dependent transmission measurements," J. Lightwave Technol. **16**(7), 1285–1294 (1998).
16. A. Zadok, N. Simon, and A. Eyal, "The dependence of the output stokes parameters on the state of an arbitrarily located polarization controller in PMD mitigation schemes," J. Lightwave Technol. **22**(6), 1533–1538 (2004).
17. M. Petersson, H. Sunnerud, M. Karlsson, and B. E. Olsson, "Performance monitoring in optical networks using stokes parameters," IEEE Photon. Technol. Lett. **16**(2), 686–688 (2004).
18. W. Xiang, and A. M. Weiner, Digest of the LEOS Summer Topical Meetings, "Fast multi-wavelength polarimeter for polarization mode dispersion compensation systems," WB2.4/67–173.

#123233 - $15.00 USD Received 25 Jan 2010; accepted 21 Feb 2010; published 16 Mar 2010

19. X. S. Yao, L. Yan, and Y. Shi, "Highly repeatable all-solid-state polarization-state generator," Opt. Lett. **30**(11), 1324–1326 (2005).
20. X. S. Yao, X. Chen, and L. Yan, "Self-calibrating binary polarization analyzer," Opt. Lett. **31**(13), 1948–1950 (2006).
21. B. L. Heffner, "Automated measurement of polarization mode dispersion using Jones matrix eigenanalysis," IEEE Photon. Technol. Lett. **4**(9), 1066–1069 (1992).
22. B. L. Heffner, "Deterministic, Analytically Complete Measurement of Polarization-Dependent Transmission Through Optical Devices," IEEE Photon. Technol. Lett. **4**(5), 451–454 (1992).
23. R. M. Craig, S. L. Gilbert, and P. D. Hale, "High-resolution, nonmechanical approach to polarization-dependent transmission measurements," J. Lightwave Technol. **16**(7), 1285–1294 (1998).
24. H. Dong, P. Shum, M. Yan, J. Q. Zhou, G. X. Ning, Y. D. Gong, and C. Q. Wu, "Generalized Mueller matrix method for polarization mode dispersion measurement in a system with polarization-dependent loss or gain," Opt. Express **14**(12), 5067–5072 (2006).
25. P.A Williams, S.M. Etzel, J. D. Kofler and C.M Wang, "Standard Reference Material 2538 for Polarization-mode dispersion (Non-mode coupled)," NIST special publication 260–145.
26. S. M. Etzel, A. H. Rose, and C. M. Wang, "Dispersion of the temperature dependence of the retardance in $SiO_{(2)}$ and MgF(2)," Appl. Opt. **39**(31), 5796–5800 (2000).
27. J. P. Gordon, and H. Kogelnik, "PMD fundamentals: polarization mode dispersion in optical fibers," Proc. Natl. Acad. Sci. U.S.A. **97**(9), 4541–4550 (2000).
28. X. Y. Kalisky, p.168 in *The Physics and Engineering of Solid State Lasers*, (SPIE Press, Bellingham, Washington, 2005).
29. M. Born, and E. Wolf, p38-p54, in *Principles of Optics*, 7th ed. University Press, Cambridge, UK, 1999.
30. *BK7 Glass data sheet,* http://www.us.schott.com/advanced_optics/us/abbe_datasheets/datasheet_n-bk7.pdf?highlighted_text=BK7
31. Y. Shi, L. Yan, and X. S. Yao, "Automatic maximum-minimum search method for accurate PDL and DOP characterization," J. Lightwave Technol. **24**(11), 4006–4012 (2006).
32. E. Collett, Chapter 9 in Polarized Light in Fiber Optics (The PolaWave Group Lincroft, New Jersey, USA, 2003).
33. N. G. Walker, and G. R. Walker, "Polarization control for coherent communications," J. Lightwave Technol. **8**(3), 438–458 (1990).
34. Data sheet of Agilent N7788B/N7788BD optical component analyzer *http://www.home.agilent.com/agilent/redirector.jspx?action=ref&cname=AGILENT_EDITORIAL&ckey=1203309*.
35. Date sheet of Thorlabs PMD/PDL Analysis System PMD5000, *http://www.thorlabs.us/NewGroupPage9.cfm?ObjectGroup_ID=1592*.
36. B. L. Heffner, "Attosecond-resolution measurement of polarization mode dispersion in short sections of optical fiber," Opt. Lett. **18**(24), 2102–2104 (1993).
37. D. Derickson, Chap 6 in *Fiber Optic Test and Measurement* (Prentice-Hall, Upper Saddle River, New Jersey, 1998).
38. R. M. Craig, "Interlaboratory comparison of polarizationcrosstalk measurement methods in terminated high birefringence optical fiber," in *Optical Fiber Communication Conference (OFC)*, Vol. 2 of 1998 OSA Technical Digest Series (Optical Society of America, 1998), pp. 180–181.
39. D. Penninckx, and N. Beck, "Definition, meaning, and measurement of the polarization extinction ratio of fiber-based devices," Appl. Opt. **44**(36), 7773–7779 (2005).
40. S. C. Rashleigh, "Measurement of fiber birefringence by wavelength scanning: effect of dispersion," Opt. Lett. **8**(6), 336–338 (1983).
41. T. Ritari, H. Ludvigsen, M. Wegmuller, M. Legré, N. Gisin, J. Folkenberg, and M. Nielsen, "Experimental study of polarization properties of highly birefringent photonic crystal fibers," Opt. Express **12**(24), 5931–5939 (2004).
42. Corning panda PM specialty fibers, PI936, *http://www.corning.com/WorkArea/downloadasset.aspx?id=18341*

1. Introduction

As the bit rate of fiber optic communication systems increases from 10 Gbps to 40Gbps, 100Gbps, and beyond, polarization related issues have more and more of an impact on system performance [1]. Polarization related impairments such as polarization mode dispersion (PMD) [2] and polarization dependent loss (PDL) [3] degrade system performance and cause service outages. On the other hand, signals with orthogonal states of polarization can be multiplexed and demultiplexed to double the transmission rate and enable high bit-rate transmission while using smaller bandwidth [4]. Finally, coherent detection, which is critical to 40Gbps and 100Gbps systems, relies on precise polarization management [5, 6]. Consequently, the need for rapid, precise measurement of all polarization related parameters of components and systems is becoming correspondingly acute.

Until recently, optical polarization related measurements have relied on analog technologies [7], including rotating retarders [8,9], rotating polarizers [10,11], liquid crystal cells [12], phase modulators [13], and four-detector methods [14]. Such analog technologies

#123233 - $15.00 USD Received 25 Jan 2010; accepted 21 Feb 2010; published 16 Mar 2010

suffer from inherently low repeatability and require complicated compensation techniques in order to achieve high accuracy measurements. Polarization analysis based on binary ferroelectric liquid crystals was reported recently [15–18] and was shown to have certain advantages over its analog counterparts. However, its accuracy and repeatability are yet to be proved.

In a previous publication [19], we reported the development of a binary polarization state generator (PSG) capable of generating five or six particular polarization states on the Poincaré Sphere with a repeatability of better than 0.1° using binary magneto-optic (MO) polarization rotators. We subsequently reported [20] a highly accurate self-calibrating polarization state analyzer (PSA) using the same binary polarization rotators. We pointed out in [19, 20] that a PSG-PSA pair can be used to accurately measure an optical component's polarization dependent loss (PDL), polarization mode dispersion (PMD), retardation, and birefringence. In this paper, we describe in detail the setup and theory for the use of a binary PSG and PSA for component characterization, and then present experimental data to show the accuracy and repeatability of the technique. In order to determine the accuracy of our binary measurement system, we designed and fabricated several PMD and PDL artifacts with precisely known PMD and PDL values to verify our measurement results. We then performed multiple PMD and PDL measurements to determine the resolution, accuracy, and repeatability of the binary approach. With PMD, SOPMD and PDL accuracies of 2.6 fs, 1.39 ps^2, and 0.06dB, respectively; repeatabilities of 0.022 fs, 0.28 ps^2, and 0.034 dB, respectively; and resolutions of 1 fs, 0.005 ps^2 and 0.01dB, respectively, the binary technique has wide potential for applications in fiber characterization, optical component measurements, and optical component manufacturing. Finally, we describe the use of our binary measurement system for additional applications, including the measurement of polarization extinction ratio and PM fiber beat length.

2. System description

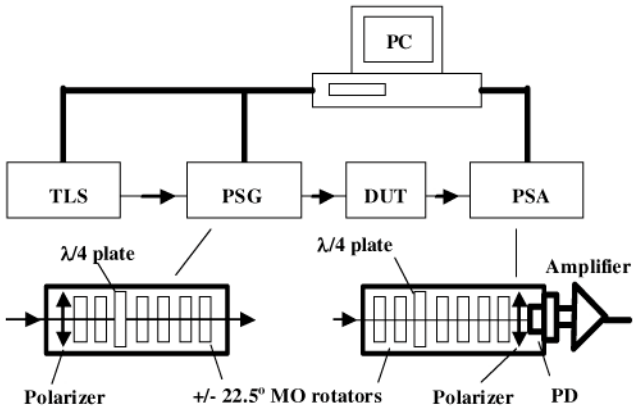

Fig. 1. The construction of a binary polarization measurement system comprised of a PSG and a PSA made with binary magneto-optic polarization rotators, a tunable laser, and a computer.

As shown in Fig. 1, the binary polarization measurement system consists of a tunable laser (TLS), a binary MO PSG, a binary MO PSA, and a control computer (PC). The device under test (DUT) is placed between the PSG and PSA. The PSG and PSA each contain 6 binary MO polarization rotators, a polarizer, and a quarter wave plate. The PSA also contains a photodetector (PD) and a signal amplification circuit. As described in [19] and [20], our MO rotators have the following attractive binary properties: when a positive magnetic field above a saturation level is applied, the rotator rotates the SOP by a precise angle θ. When a negative magnetic field beyond the saturation level is applied, the rotator rotates the SOP by precisely −θ. For the purposes of the PSG and PSA, θ is designed to be around 22.5°. Therefore, when two rotators rotate the SOP in the same direction, the net rotation is +45° or –45°. Conversely,

#123233 - $15.00 USD Received 25 Jan 2010; accepted 21 Feb 2010; published 16 Mar 2010

if the two rotators rotate the SOP in opposite directions, the net SOP rotation is zero. With the rotation directions of each rotator controlled by the PC, the PSG can generate 6 particular polarization states and the PSA can accurately measure the state of polarization (SOP) and the degree of polarization (DOP) of light entering it by analyzing voltages generated in the photodetector using Mueller Matrix analysis. As described in [20], the binary PSA can also be self-calibrated to remove inaccuracies caused by imperfections in components and workmanship, yielding extremely high measurement accuracies.

Both Jones and Mueller matrix analysis methods can be used to obtain the complete set of polarization related information of a DUT, including PMD (birefringence), PSP (orientation angle of birefringence), PDL (diattentuation), and PDL orientation angle. Other methods, such as the wavelength scanning method, can be used to obtain PMD information only. The system shown in Fig. 1 can be used to implement all of the measurement methods described above, but in this paper, we will concentrate on its use with the Jones and Mueller matrix methods to measure and calculate the complete polarization information of a DUT. We will then validate our measurement system by using it to measure specially made PMD and PDL artifacts and compare the measurement results with the theoretical values of the artifacts. Finally, we will describe the use of this system for other applications, including the measurements of the polarization extinction ratio (PER) of a polarization maintaining (PM) fiber, the stress in a PM connector, and the beat length of a PM fiber.

3. Theoretical background

3.1 Jones Matrix eigenanalysis method (JME)

Obtaining the Jones Transfer Matrix: Generally, the polarization transfer matrix of an optical device under test (DUT) can be described by a 2x2 complex Jones transfer matrix **Γ**, and the input and output polarization states are related by [21]

$$\begin{bmatrix} J_x^{PSA} \\ J_y^{PSA} \end{bmatrix} = c^* \begin{bmatrix} \Gamma_{00} & \Gamma_{01} \\ \Gamma_{10} & 1 \end{bmatrix} \begin{bmatrix} J_x^{PSG} \\ J_y^{PSG} \end{bmatrix}, \tag{1}$$

where J^{PSG} is the normalized Jones vector of the light output generated by the PSG, J^{PSA} is the normalized Jones vector of the light measured by the PSA, and c* is a complex constant related to the absolute amplitude and absolute phase of the light wave. Note that the ratio of $\frac{J_x^{PSA}}{J_y^{PSA}}$ is

$$\frac{J_x^{PSA}}{J_y^{PSA}} = \frac{\Gamma_{00}^J J_x^{PSG} + \Gamma_{01}^J J_y^{PSG}}{\Gamma_{10}^J J_x^{PSG} + J_y^{PSG}} \tag{2}$$

and is independent of the constant c*. If three sets of vectors $\mathbf{J}^{PSG}$ and $\mathbf{J}^{PSA}$ are generated and measured, we can obtain the following equations:

$$\begin{aligned} J_{0,x}^{PSG} J_{0,y}^{PSA} \Gamma_{00}^J + J_{0,y}^{PSG} J_{0,y}^{PSA} \Gamma_{01}^J - J_{0,x}^{PSG} J_{0,x}^{PSA} \Gamma_{10}^J &= J_{0,y}^{PSG} J_{0,x}^{PSA} \\ J_{1,x}^{PSG} J_{1,y}^{PSA} \Gamma_{00}^J + J_{1,y}^{PSG} J_{1,y}^{PSA} \Gamma_{01}^J - J_{1,x}^{PSG} J_{1,x}^{PSA} \Gamma_{10}^J &= J_{1,y}^{PSG} J_{1,x}^{PSA} \\ J_{2,x}^{PSG} J_{2,y}^{PSA} \Gamma_{00}^J + J_{2,y}^{PSG} J_{2,y}^{PSA} \Gamma_{01}^J - J_{2,x}^{PSG} J_{2,x}^{PSA} \Gamma_{10}^J &= J_{2,y}^{PSG} J_{2,x}^{PSA} \end{aligned} \tag{3}$$

Let $k_{i,0} = J_{i,x}^{PSG} J_{i,y}^{PSA}$, $k_{i,1} = J_{i,y}^{PSG} J_{i,y}^{PSA}$, $k_{i,2} = -J_{i,x}^{PSG} J_{i,x}^{PSA}$, and $k_{i,3} = J_{i,y}^{PSG} J_{i,x}^{PSA}$ (i=0,1,2), then Eq. (3) can be simplified to

#123233 - $15.00 USD Received 25 Jan 2010; accepted 21 Feb 2010; published 16 Mar 2010

$$\begin{aligned} k_{00}\Gamma_{00}^{J} + k_{01}\Gamma_{01}^{J} + k_{02}\Gamma_{10}^{J} &= k_{03} \\ k_{10}\Gamma_{00}^{J} + k_{11}\Gamma_{01}^{J} + k_{12}\Gamma_{10}^{J} &= k_{13} \\ k_{20}\Gamma_{00}^{J} + k_{21}\Gamma_{01}^{J} + k_{22}\Gamma_{10}^{J} &= k_{23} \end{aligned}, \quad (4)$$

and the Jones transfer matrix **Γ** of the DUT can be easily calculated using

$$\Gamma_{00} = \frac{\begin{vmatrix} k_{03} & k_{01} & k_{02} \\ k_{13} & k_{11} & k_{12} \\ k_{23} & k_{21} & k_{22} \end{vmatrix}}{\begin{vmatrix} k_{00} & k_{01} & k_{02} \\ k_{10} & k_{11} & k_{12} \\ k_{20} & k_{21} & k_{22} \end{vmatrix}}, \quad \Gamma_{01} = \frac{\begin{vmatrix} k_{00} & k_{03} & k_{02} \\ k_{10} & k_{13} & k_{12} \\ k_{20} & k_{23} & k_{22} \end{vmatrix}}{\begin{vmatrix} k_{00} & k_{01} & k_{02} \\ k_{10} & k_{11} & k_{12} \\ k_{20} & k_{21} & k_{22} \end{vmatrix}}, \quad \Gamma_{10} = \frac{\begin{vmatrix} k_{00} & k_{01} & k_{03} \\ k_{10} & k_{11} & k_{13} \\ k_{20} & k_{21} & k_{23} \end{vmatrix}}{\begin{vmatrix} k_{00} & k_{01} & k_{02} \\ k_{10} & k_{11} & k_{12} \\ k_{20} & k_{21} & k_{22} \end{vmatrix}} \quad (5)$$

It is important to note that in Eqs. (3) to (5), the three polarization states generated by the PSG are not specified in our analysis. Any three non-degenerate SOPs generated by the PSG can be used to obtain the 2x2 complex Jones transfer matrix **Γ.** The lack of restrictions on the SOPs used eliminates the accuracy requirement for the PSG and makes our system less susceptible to variations caused by the wavelength and temperature dependences of the PSG. By comparison, other Jones Matrix analysis implementations [21] require precise polarization state generation at specific points on the Poincaré Sphere (0, 45, and 90 degrees), rendering the measurement system more susceptible to imperfections in the PSG.

Obtaining PDL: For a given optical frequency, the PDL of a DUT can be calculated as [22, 23]:

$$PDL = 10 * \log\left|\frac{r_1}{r_2}\right|, \quad (6)$$

where $r_{1,2} = \frac{m_{11}+m_{22}}{2} \pm \sqrt{(\frac{m_{11}+m_{22}}{2})^2 - m_{11}m_{22} + m_{12}m_{21}}$ are the eigenvalues of the matrix M $=(\mathbf{\Gamma}^{-1})^* \bullet \mathbf{\Gamma} = \begin{bmatrix} m_{11} & m_{12} \\ m_{21} & m_{22} \end{bmatrix}$, $\mathbf{\Gamma}^{-1}$ is the transpose of Jones transfer matrix **Γ,** and the star * indicates the complex conjugate.

Obtaining PMD [21]: For two adjacent optical frequencies, define a matrix:

$$T(\Delta\omega) = \Gamma(\omega_2)\Gamma(\omega_1)^{-1} \quad (7)$$

The complex eigenvectors ρ_s and ρ_f of matrix $T(\Delta\omega)$ are the fast and slow principal states of polarization of the DUT, and the differential group delay (**DGD**) $\tau(\omega)$ can be calculated from

$$\tau(\omega) = \left|\tau_s - \tau_f\right| = \left|\frac{Arg(\rho_s/\rho_f)}{\omega_1 - \omega_2}\right|, \quad (8)$$

where

$$\omega = \frac{\omega_1 + \omega_2}{2} \quad (9)$$

and $Arg(\rho_s/\rho_f)$ stands for the phase angle of ρ_s/ρ_f . The wavelength dependent PMD vector $\overrightarrow{W}$ can be defined as

#123233 - $15.00 USD Received 25 Jan 2010; accepted 21 Feb 2010; published 16 Mar 2010

$$\overrightarrow{W}(\omega) = \tau(\omega)\vec{q}(\omega) \tag{10}$$

where $\vec{q}(\omega)$ is the unit vector of the fast principal state of polarization. The second-order PMD, defined as the frequency derivative of the PMD vector $\overrightarrow{W}$, can be calculated as

$$SOPMD = \frac{d\vec{W}(\omega)}{d\omega} = \frac{d\tau(\omega)}{d\omega}\vec{q}(\omega) + \tau(\omega)\frac{d\vec{q}(\omega)}{d\omega} \tag{11}$$

3.2 Mueller matrix measurement method (MMM)

Obtaining the Mueller matrix: Let the Stokes vector of the ith output of the PSG be

$$S_i^{PSG} = \begin{pmatrix} S_{0i}^{PSG} \\ S_{1i}^{PSG} \\ S_{2i}^{PSG} \\ S_{3i}^{PSG} \end{pmatrix}, \tag{12}$$

The corresponding Stokes vectors measured by the PSA after the light passes through the DUT are related to Mueller Matrix M by:

$$S_i^{PSA} = \begin{pmatrix} S_{0i}^{PSA} \\ S_{1i}^{PSA} \\ S_{2i}^{PSA} \\ S_{3i}^{PSA} \end{pmatrix} = \begin{pmatrix} m_{00} & m_{01} & m_{02} & m_{03} \\ m_{10} & m_{11} & m_{12} & m_{13} \\ m_{20} & m_{21} & m_{22} & m_{23} \\ m_{30} & m_{31} & m_{32} & m_{33} \end{pmatrix} \begin{pmatrix} S_{0i}^{PSG} \\ S_{1i}^{PSG} \\ S_{2i}^{PSG} \\ S_{3i}^{PSG} \end{pmatrix} \tag{13}$$

At least 4 non-degenerate SOPs must be generated by the PSG and analyzed by the PSA to completely determine Mueller Matrix M by solving Eq. (13). In such a case, i = 0, 1, 2, 3 in Eqs. (12) and (13). However, for higher accuracies, we require that as many as 6 non-degenerate SOPs be generated by the PSG and analyzed by the PSA, so that i = 0, 1, 2…5. Define a new matrix $\mathbf{S}^{\mathrm{PSA}}$ as

$$\begin{aligned} \mathrm{S}^{\mathrm{PSA}} &= \begin{pmatrix} S_{00}^{PSA} & S_{01}^{PSA} & S_{02}^{PSA} & S_{03}^{PSA} & S_{04}^{PSA} & S_{05}^{PSA} \\ S_{10}^{PSA} & S_{11}^{PSA} & S_{12}^{PSA} & S_{13}^{PSA} & S_{14}^{PSA} & S_{15}^{PSA} \\ S_{20}^{PSA} & S_{21}^{PSA} & S_{22}^{PSA} & S_{23}^{PSA} & S_{24}^{PSA} & S_{25}^{PSA} \\ S_{30}^{PSA} & S_{31}^{PSA} & S_{32}^{PSA} & S_{33}^{PSA} & S_{34}^{PSA} & S_{35}^{PSA} \end{pmatrix} \\ &= \begin{pmatrix} m_{00} & m_{01} & m_{02} & m_{03} \\ m_{10} & m_{11} & m_{12} & m_{13} \\ m_{20} & m_{21} & m_{22} & m_{23} \\ m_{30} & m_{31} & m_{32} & m_{33} \end{pmatrix} \begin{pmatrix} S_{00}^{PSG} & S_{01}^{PSG} & S_{02}^{PSG} & S_{03}^{PSG} & S_{04}^{PSG} & S_{05}^{PSG} \\ S_{10}^{PSG} & S_{11}^{PSG} & S_{12}^{PSG} & S_{13}^{PSG} & S_{14}^{PSG} & S_{15}^{PSG} \\ S_{20}^{PSG} & S_{21}^{PSG} & S_{22}^{PSG} & S_{23}^{PSG} & S_{24}^{PSG} & S_{25}^{PSG} \\ S_{30}^{PSG} & S_{31}^{PSG} & S_{32}^{PSG} & S_{33}^{PSG} & S_{34}^{PSG} & S_{35}^{PSG} \end{pmatrix} \\ &= \mathrm{M} \bullet \mathrm{S}^{PSG} \end{aligned} \tag{14}$$

Consequently, the Mueller matrix of the DUT can be obtained from

$$\mathrm{M} = \mathrm{S}^{\mathrm{PSA}} \bullet (\mathrm{S}^{\mathrm{PSG}})^{T} \bullet [\mathrm{S}^{\mathrm{PSG}} \bullet (\mathrm{S}^{\mathrm{PSG}})^{T}]^{-1} \tag{15}$$

where $(\mathbf{S}^{\mathrm{PSG}})^{\mathrm{T}}$ is the transpose of matrix $\mathbf{S}^{\mathrm{PSG}}$.

Obtaining PDL: For a given optical frequency, the PDL of a DUT can be obtained [23] from

#123233 - $15.00 USD Received 25 Jan 2010; accepted 21 Feb 2010; published 16 Mar 2010

$$PDL = -10 \times \log(\frac{P_{Min}}{P_{Max}}) = -10 \times \log \frac{m_{00} - \sqrt{m_{01}^2 + m_{02}^2 + m_{03}^2}}{m_{00} + \sqrt{m_{01}^2 + m_{02}^2 + m_{03}^2}} \quad (16)$$

Obtaining PMD: For two adjacent optical frequencies, define a matrix

$$M_{\Delta}(\overline{\omega}) = M(\omega_2)M^{-1}(\omega_1) \quad (17)$$

The complex PMD vector $\vec{W} = \vec{\Omega} + i\vec{\Lambda}$ can be found from the matrix $\mathbf{M}_{\Delta}$ [24], where $\vec{\Omega}$ and $\vec{\Lambda}$ are the real and complex components of $\vec{W}$, respectively. The expression for $\vec{W}$ is rather complicated, so we will obtain the result numerically. The DGD and PSP vectors can be calculated using

$$DGD = \mathrm{Re}(\sqrt{\vec{W} \bullet \vec{W}}) \quad (18)$$

$$q(\omega)_{\pm} = \frac{\pm\vec{\Omega} + \vec{\Omega} \otimes \vec{\Lambda}}{\vec{\Omega} \bullet \vec{\Lambda}} \quad (19)$$

where q_+ and q_- are the unit vectors of the slow and fast PSP, respectively. The symbol "$\otimes$" in Eq. (19) stands for cross product, and "$\bullet$" stands for inner product. As with the case using the JME method, the second order PMD can be calculated numerically using Eq. (11), but with q replaced by q_-.

4. PMD and PDL artifacts

To validate the accuracy of our binary polarization measurement technique, PMD and PDL artifacts with precise PMD and PDL values were required. We fabricated such PMD and PDL standards, shown in Fig. 2, with PMD and PDL values defined by quantities that are precisely known, as described below.

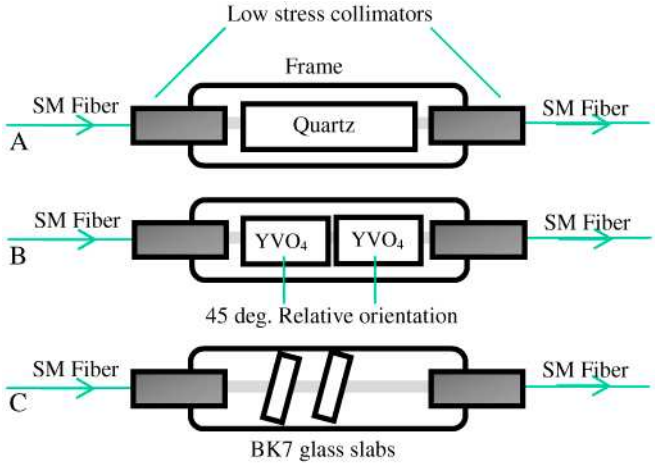

Fig. 2. Schematic design of DGD, SOPMD, and PDL artifacts. (A) Precision wavelength independent DGD artifact. (B) Wavelength independent combined DGD and SOPMD artifact. The birefringence axes of two YVO_4 crystals are oriented 45° from each other. (C) Wavelength independent PDL artifact. Fused silica, BK7 or other types of glass can be used to make the artifact.

4.1 DGD artifacts

1st order PMD (DGD) artifacts were constructed using quartz crystals of precise lengths, whose DGD values can be obtained by:

#123233 - $15.00 USD Received 25 Jan 2010; accepted 21 Feb 2010; published 16 Mar 2010

$$DGD = \Delta n_g L / c \tag{20}$$

where L is the length of the quartz crystal, c is the speed of light in vacuum, and Δn_g is the group birefringence defined as:

$$\Delta n_g = \Delta n - \lambda \frac{d\Delta n}{d\lambda} \tag{21}$$

In Eq. (21), Δn is the phase birefringence and λ is the wavelength in vacuum.

Quartz is the most well-known birefringent crystal, with birefringences at different wavelengths precisely known to an accuracy of about 0.25% [25]. In addition, quartz crystals have excellent temperature stability with respect to both dimension and birefringence, with an extremely low temperature coefficient of 1.232×10^{-4}/°C [9, 26] for total retardation. Furthermore, the processes for cutting and polishing quartz crystals are mature, and the dimensional tolerance is better than 10μm. Finally, quartz crystals are environmentally stable and their physical properties are generally not affected by aging. We enclosed a quartz crystal of 20mm length in a 27 x 6 x 6 (mm) stainless steel package, pigtailed using a pair of low-stress fiber collimators, as shown in Fig. 2(A). The collimators are soldered to the stainless steel package using a standard process for making telecom grade fiber optic components with high environmental and long-term stabilities. The use of low-stress fiber collimators is necessary to minimize stress-induced birefringence and its effect on the overall DGD accuracy. As a result, the overall DGD accuracy at 1550nm is better than 2.03 fs within a temperature range of 23±5 °C at all times, as shown in Table 1. This DGD artifact can therefore be used as a "golden" calibration standard for calibrating different PMD measurement instruments.

Table 1. Summary of sources of DGD uncertainty in a quartz DGD artifact*

Uncertainty Source	Uncertainty	Artifact DGD Uncertainty
Δn_g	0.000026 [25]	$\sigma_{\Delta ng}$ =1.7fs
Length of quartz crystal	±10μm	σ_L=0.3fs
Temperature of crystal	±5°C	σ_T=0.4fs
Pigtail birefringence	±1fs	$\sigma_{Pigtail}$=1.0fs
Total uncertainty $\sigma_{DGD} = \sqrt{\sigma_{\Delta n_g}^2 + \sigma_L^2 + \sigma_T^2 + \sigma_{Pigtail}^2}$ =2.03fs		

* The artifact is made with a 20mm long quartz crystal with a DGD value of 627.7fs at 1550nm

4.2 SOPMD artifacts

Wavelength independent second order PMD (SOPMD) artifacts were constructed by cascading two birefringent YVO_4 crystals with their birefringent axes oriented 45 degrees from each other, as shown in Fig. 2(B). The SOPMD can be calculated as [27]:

$$SOPMD = \tau_1 \tau_1 \sin(2\theta) \tag{22a}$$

The corresponding DGD is

$$DGD = \sqrt{\tau_1^2 + \tau_1^2 + 2\tau_1 \tau_2 \cos(2\theta)} \tag{22b}$$

where θ is the relative orientation angle between the two crystal sections. Like quartz, YVO_4 is a commonly used birefringent crystal with precisely known birefringences at different wavelengths. However, with a birefringence about 23 times larger than that of a quartz crystal, it is a better choice for making compact SOPMD artifacts with practical SOPMD values. YVO_4 also has reasonable temperature stability with respect to both dimensions and

#123233 - $15.00 USD Received 25 Jan 2010; accepted 21 Feb 2010; published 16 Mar 2010

birefringence, with a fairly low thermal optic coefficient (<1x10^{-5}/°C) [28]. Like quartz crystals, YVO_4 crystal elements can be made with a dimensional tolerance better than 10μm and are environmentally stable, with their physical properties unaffected by aging. We used the same packaging materials and process used for the DGD artifacts to assemble and pigtail SOPMD artifacts of different SOPMD values. The relative orientation angle can be readily controlled to within ±1 degree. The resulting accuracy is 0.86 ps^2 for an artifact made by cascading two 16mm YVO_4 crystals (see Table 2); its anticipated DGD and SOPMD values are 16.15ps and 130.2 ps^{2,} respectively.

Table 2. Summary of sources of uncertainty in a YVO_4 SOPMD artifact*

Uncertainty Source	Uncertainty	Artifact SOPMD Uncertainty
DGD of Crystal 1	0.04ps	σ_{DGD1}=0.46ps^2
DGD of Crystal 2	0.04ps	$\sigma_{DGD2=}$0.46ps^2
Temperature (±5°C)	5x10^{-5} /°C	σ_T=0.04ps^2
Pigtail birefringence	0.002ps	$\sigma_{Pigtail}$=0.032ps^2
Relative orientation angle	±1degree	$\sigma_{Orientation}$=0.32ps^2
Total uncertainty $= \sqrt{\sigma^2_{\Delta DGD1} + \sigma^2_{\Delta DGD2} + \sigma^2_T + \sigma^2_{Pigtail} + \sigma^2_{Orientation}}$ =0.73ps^2		

*The artifact is constructed with two 16mm YVO_4 crystals cascaded with a 45 degree orientation with respect to each other. The anticipated DGD and SOPMD values are 16.15ps and 130.2ps^2, respectively

4.3 PDL artifacts

We also designed and fabricated PDL artifacts using BK7 glass slabs oriented at different angles with respect to the direction of incident light, as shown in Fig. 2(C). Because the transmittances of the p- and s-components are different and are wavelength independent, the transmitted light will have a wavelength independent polarization dependent loss (diattenuation). The transmittance of the p- and s- polarization components at an interface of an optical slab can be readily calculated using Fresnel equations [29]:

$$T_p = \frac{\sin 2\theta_i \sin 2\theta_t}{\sin^2(\theta_i + \theta_t)\cos^2(\theta_i - \theta_t)} \tag{23}$$

$$T_s = \frac{\sin 2\theta_i \sin 2\theta_t}{\sin^2(\theta_i + \theta_t)}, \tag{24}$$

where θ_i and θ_t are the incidence and refraction angles, and are related by Snell's Law: $\sin(\theta_i)/\sin(\theta_t)=n_i/n_t$. The corresponding PDL can be calculated using

$$PDL = \left| 10\log(\frac{T_p}{T_s}) \right| = -10\log\left[\cos^2(\theta_i - \theta_t)\right] \tag{25}$$

Because each slab has front and rear surfaces, the PDL value of a PDL artifact containing a single slab of BK7 is the summation of the PDL values from both surfaces. Similarly, the PDL value of a PDL artifact made with multiple slabs is the summation of the PDL values of all slabs used in the artifact. We chose BK7 glass [30] for its temperature stability, dimensional stability, and ease of fabrication. In order to minimize the interference of light reflected from the front and rear surfaces, the rear surface is polished at a 0.5° tilt angle with respect to the front surface. Table 3 summarizes the PDL uncertainties caused by different factors. Clearly, the largest uncertainty factor is the incidence angle to the slab.

#123233 - $15.00 USD Received 25 Jan 2010; accepted 21 Feb 2010; published 16 Mar 2010

Table 3. Summary of uncertainty sources in a PDL artifact

Uncertainty Source	Uncertainty	Artifact PDL Uncertainty	
		0.4-dB artifact *	**2-dB artifact***
Incidence angle tolerance	0.5°	0.013dB	0.050dB
Tolerance of angle between front and rear surfaces	0.1°	0.002dB	0.014dB
Tolerance of index of BK7 slab	<0.001	0.0012dB	0.004dB
Temperature [30]	±5°C ($\Delta n=\pm 1.2\times10^{-5}$)	$<1.6\times10^{-5}$	0.00005dB
Total uncertainty:		**0.013dB**	**0.052dB**

The nominal incidence angles are 33.92° and 62.93°, respectively, for the 0.4-dB and 2-dB artifacts.

As shown in Table 3, the largest contributions to the total uncertainty are caused by the tolerances of the incidence angle and the angle between the slab's two surfaces. These are fixed once the fiber collimators are soldered to the case, as shown in Fig. 2. To counter their effect, we calibrated the artifacts' PDL values using the maximum and minimum search method [31]. Specifically, we searched for the maximum and minimum output powers from an artifact while varying the input polarization. The power difference in dB is the PDL value of the artifact. The calibration results are 0.387±0.005dB for a nominally 0.4-dB artifact and 1.959±0.010dB for a nominally 2-dB artifact. For the calibration, we used a highly stable laser source (Agilent 81640A), a high quality polarization controller with extremely low activation loss (General Photonics Model PCS-4X with activation loss less than 0.005 dB) and a polarization insensitive power meter built with an integrated optical sphere (ILX Lightwave FPM-8210). Once calibrated, the PDL variation due to temperature variation is negligible, as shown in Table 3.

5. Experimental results

5.1 PMD measurement resolution

To characterize the resolution of our measurement system, we measured the PMD value of a piece of single mode fiber. We placed a 2-cm section of the bare fiber in a fiber squeezer (General Photonics' fiber squeezer polarization controller, PLC-003) to induce a small amount of birefringence or PMD in the fiber via the photo-elastic effect, and then measured the PMD value of the fiber as the pressure on the fiber was increased. As shown in Fig. 3(A), as the pressure on the fiber section increases, the SOP traces out a circle on the Poincaré Sphere [32, 33]. A complete circle corresponds to a 2π retardation caused by pressure induced birefringence or, at a wavelength of 1550nm, a DGD of 5.2 fs. Therefore, the pressure induced DGD value can be approximated by counting the SOP revolutions as the pressure on the fiber section is increased using the fiber squeezer. Figure 3(B) shows the DGD as a function of wavelength, measured with the binary system described in Fig. 1 using the Jones Matrix method for two cases: one with no applied pressure and the other with an applied pressure corresponding to a SOP rotation angle of 2π. It is evident that our system can easily distinguish PMD value changes as small as 1 fs. The measured DGD of 0.82fs with no applied pressure is the combination of the DGD of the fiber itself and the noise floor of the measurement system. It can therefore be concluded that the DGD measurement resolution of our measurement system is better than 1 fs. The same resolution is also obtained when the Mueller Matrix method is used. Figure 3(C) shows the pressure induced DGD as a function of SOP rotation angle. The dashed line is the DGD obtained from the SOP rotation angle, while the black dots represent the DGD obtained with our measurement system. The measured DGD shows good agreement with that obtained by SOP angle counting. Again, a measurement resolution of less than 1 fs is clearly demonstrated.

#123233 - $15.00 USD Received 25 Jan 2010; accepted 21 Feb 2010; published 16 Mar 2010

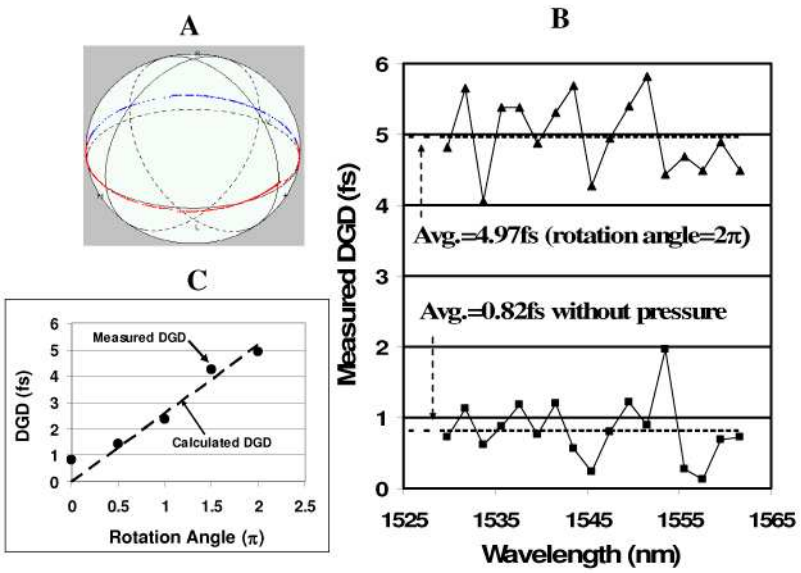

Fig. 3. (A) SOP evolution as the pressure on the fiber is increased. (B) Experimental results illustrating the PMD measurement resolution of the measurement system using binary MO polarization rotators. (C) Pressure induced DGD as a function of SOP evolution angles at 1550 nm. Black dots: DGD obtained with binary measurement system. Dashed line: DGD obtained by SOP angle counting. A PMD measurement resolution of 1 fs is clearly demonstrated in both B and C. In addition, the measurement accuracy is also confirmed by the rotation angle of the SOP: the 5.2 fs DGD corresponds to a total SOP rotation angle of 2π at 1550 nm.

5.2 DGD and SOPMD measurements

We constructed a DGD artifact using a 20 mm long quartz crystal and measured its DGD value using the binary system described in Fig. 1. The DGD value calculated from Eqs. (20) and (21) and birefringence data at 1550 nm from [25] is 627.7fs±2.03 fs (see Table 1). The measured DGD values, averaged over the c-band, using the Jones matrix eigenanalysis (JME) and Mueller matrix measurement (MMM) methods are 627.0 fs and 628.1 fs, respectively. The measured DGD as a function of wavelength is shown in Fig. 4. The wavelength variations of the measured DGD are ± 2.75fs and ±2.93fs, respectively, obtained with the JME and MMM methods. As shown in Fig. 4, our measurement system can resolve SOPMD values as small as 0.001 ps^2. However, since the largest measured SOPMD value is 0.004 ps^2 for a DGD artifact with a theoretical SOPMD value of zero ps^2, we can conservatively conclude that our measurement system has a SOPMD resolution of 0.005 ps^2. This high resolution reflects the excellent repeatability of our binary PSG and the resolution of our binary PSA used in the system.

#123233 - $15.00 USD Received 25 Jan 2010; accepted 21 Feb 2010; published 16 Mar 2010

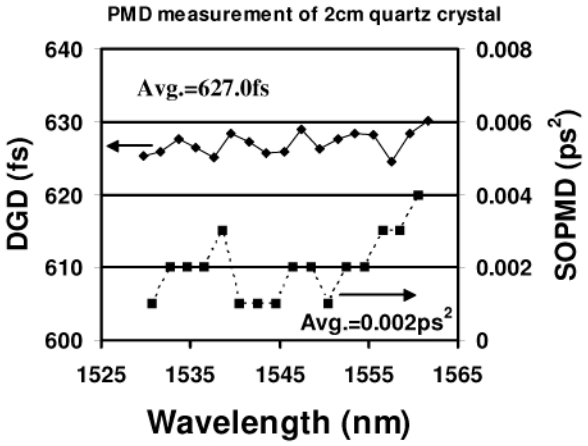

Fig. 4. 1st and 2nd order PMD of a 2-cm quartz crystal DGD artifact (calculated DGD=627.7fs), measured with Jones Matrix Eigenanalysis method using 2 nm wavelength step. Similar results are obtained with MMM method.

We constructed another PMD artifact by cascading two YVO_4 crystals of 16mm length with a 45 degree relative orientation angle, as described in Section 4.2. The DGD values of the two crystals, measured with the binary measurement system described in Fig. 1, are 11.410 ps and 11.416 ps, respectively. The expected DGD and SOPMD values of the PMD artifact are 16.14 ps and 130.2 ps^2, calculated from Eq. (22). As shown in Fig. 5, using the same measurement system, the measured DGD and SOPMD are 16.06 ps and 127.5 ps^2, respectively, using Jones matrix analysis, and 16.07 ps and 130.2 ps^2, respectively, using the Mueller Matrix Method. The corresponding DGD and SOPMD deviations of the measurement from the theoretical DGD and SOPMD values of the artifacts are 0.08 ps and 2.7 ps^2 using the Jones Matrix and 0.07 ps and <0.01 ps^2 using the Mueller Matrix Method. Clearly, the Mueller Matrix Method has a smaller PMD measurement deviation than the Jones Matrix Method for the PMD range tested. In addition, as can be seen in Section 5.4, the Mueller Matrix Method also has better measurement repeatability than the Jones Matrix Method.

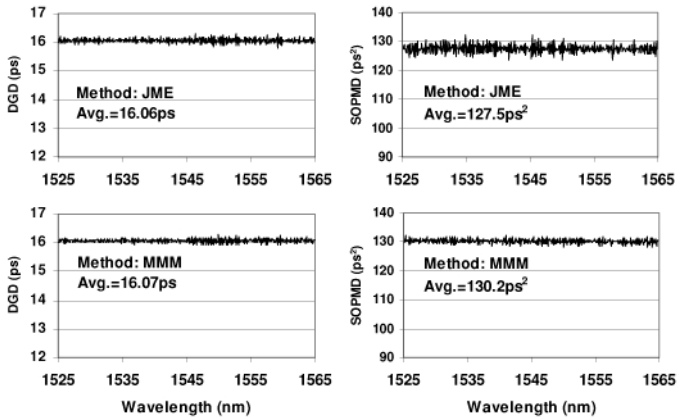

Fig. 5. DGD and SOPMD measurement results for a PMD artifact made from two 16 mm long YVO_4 crystals with a relative orientation angle of 45 degrees. (A) and (B) DGD values vs. wavelength obtained using JME and MMM methods, respectively. (C) and (D) SOPMD values vs. wavelength obtained using JME and MMM methods, respectively.

#123233 - $15.00 USD Received 25 Jan 2010; accepted 21 Feb 2010; published 16 Mar 2010

5.3 PDL measurement

We also constructed two PDL artifacts using the method described in Section 4.3. The calibrated PDL values are 1.959±0.01 dB and 0.387±0.005 dB, respectively, as shown in Section 4.3. Their PDL wavelength dependences, measured using our binary system, are shown in Fig. 6. The average measured PDL values of the two artifacts are 1.964 dB and 0.375 dB, respectively, using the Mueller matrix method, and 2.01dB and 0.416dB, respectively, using the Jones matrix method. As can be seen in Fig. 6, the values measured using the two methods are slightly different, and those measured with the Mueller matrix method show less wavelength variation. As shown in the next section, the Mueller matrix method also has better measurement repeatability. This is because the Mueller matrix method relies on power measurement, while the JME method is based on SOP measurement. As a result, the Mueller matrix method generally has better accuracy and repeatability (as shown in the next section) than the JME method for low PDL measurement because power measurement generally has better accuracy and repeatability than SOP measurement.

As can be seen from Fig. 6, the fluctuations in the measured PDL vs. wavelength values are about ±0.03dB for the Jones matrix method and ±0.005dB for the Mueller matrix method. Theoretically, the artifact's PDL should be wavelength independent. The observed fluctuation is mainly due to system noise and the wavelength dependence of the fiber pigtail's PDL vector, because the total PDL is the vector summation of the PDL of the artifact and its fiber pigtails. Based on these results, the worst-case PDL measurement resolution should be better than 0.01dB for the Mueller matrix method and 0.06dB for the Jones matrix method.

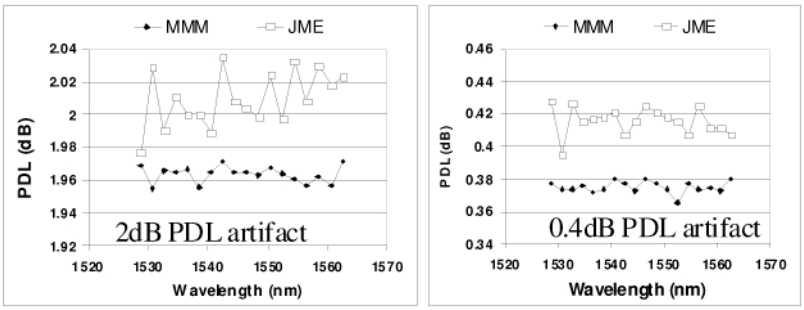

Fig. 6. Measured PDL as a function of wavelength using the JME and MMM methods. (A) PDL vs. wavelength of a "2dB" artifact, and (B) PDL vs. wavelength of a "0.4 dB" artifact. PDL obtained using MMM method has much less wavelength variation than that obtained using JME method.

5.4 Repeatability measurements and Accuracy determination

In order to determine the repeatability of our measurement system, we measured the PMD and PDL artifacts multiple times. The results are listed in Table 4. The Mueller Matrix Method data are shown to have better repeatability and accuracy than the corresponding Jones Matrix Method data; therefore, we will use Mueller Matrix results to determine the accuracy and repeatability of our measurement system. It is evident that our binary measurement system has a remarkable DGD repeatability of 0.022 fs for a 627.7 fs DGD artifact, a SOPMD repeatability of 0.28 ps^2 for a 130.2 ps^2 SOPMD artifact, a PDL repeatability of 0.041dB for a 2-dB PDL artifact, and a PDL repeatability of 0.034dB for a 0.4-dB PDL artifact, measured using the Mueller Matrix Method. Note that the DGD repeatability of our binary system is more than 100 times better than those of commercially available systems on the market [34, 35]. No published repeatability data for SOPMD measurement were found for either research or commercial measurement systems.

B. L. Heffner reported a DGD repeatability of about 0.05 fs for the measurement of an 11.423 fs quartz slab, where the measured DGD was averaged over a 1304 nm to 1540 nm range [36]. However, such a large wavelength range is difficult to obtain for practical use. By

#123233 - $15.00 USD Received 25 Jan 2010; accepted 21 Feb 2010; published 16 Mar 2010

contrast, our DGD repeatability of 0.022 fs for a 627.7 fs artifact was obtained by averaging data only from 1528nm to 1563nm, a wavelength range well within the tuning range of a commercially available tunable laser.

Note that the total PDL vector of a device under test is the vector summation of the PDL vectors of all components in the measurement setup, including connectors, fiber pigtails, and the DUT itself. The positions of the fiber pigtails determine the relative orientation of the PDL vectors involved, and hence affect the total PDL values. During measurement, we arranged the fiber pigtails of the PDL artifacts in different positions to account for PDL variation caused by the residual PDL values of the fiber pigtails and connectors. The measurement results therefore include these residual PDL contributions.

As discussed in Section 4, the 2-cm quartz DGD artifact has a "standard" DGD value of 627.7±2.03 fs (see Table 1). The worst deviations between the measured and standard DGD values are −0.70 fs and 0.41 fs, measured using JME and MMM, respectively. These deviations are well within the uncertainty range of the DGD artifact. Therefore, the absolute DGD measurement accuracies are determined to be better than |2.03fs|+|−0.68fs|+|0.39fs|=3.1fs for the JME method, and |2.03fs|+|0.41fs|+|0.19fs|=2.6fs for the MMM method, where 0.39 fs and 0.19 fs are the DGD measurement repeatabilities of our system when JME and MMM analysis methods, respectively, are used, as shown in Table 4. Note that the largest contribution to the inaccuracy is not from our measurement system itself, but from the artifact's DGD value uncertainty (2.03 fs). A much higher measurement accuracy might be claimed if an artifact with a much tighter DGD value tolerance were available. Nevertheless, it is also important to point out that the DGD measurement accuracy of our measurement system is more than 10 times better than those of commercial PMD measurement systems on the market [34].

In order to verify the measurement uniformity of our measurement method, we measured the same DGD artifact using three identical measurement systems built according to the design shown in Fig. 1, using three different PSG-PSA pairs and three different tunable lasers. The measured DGD values are 628.1 fs, 627.7 fs and 629.0 fs. The spread is well within the artifact's DGD range of 627.7 ±2.03fs.

The SOPMD artifact has a "standard" SOPMD value of 130.3±0.73 ps^2 (see Table 2). The worst measured result deviates by −2.01ps^2 and 0.38 ps^2 from the standard value when JME and MMM analysis methods, respectively, are used. Consequently, the worst-case absolute accuracy for SOPMD measurement using our system can be estimated to be |0.73 ps^2|+|−2.01 ps^2|+|1.35 ps^2|=4.18ps^2 using the JME method, and |0.73 ps^2|+|0.38 ps^2|+|0.28 ps^2|=1.39ps^2 using the MMM method, where 1.35 ps^2 and 0.28 ps^2 are the corresponding measurement repeatabilities of the two methods, as shown in Table 4. To the best of the authors' knowledge, this SOPMD measurement accuracy of 1.39 ps^2 represents the highest reported SOPMD accuracy to date.

Accuracy estimations similar to those described above for DGD and SOPMD yield a PDL measurement accuracy better than 0.223dB (JME) and 0.074dB (MMM) for the 2-dB PDL artifact, and 0.17dB (JME) and 0.06dB (MMM) for the 0.4-dB artifact.

As previously pointed out, our system generally has better accuracy and repeatability using the MMM method; therefore, we will use MMM analysis method results to determine the performance of our measurement system. We therefore conclude that our binary measurement system has DGD, SOPMD, and PDL accuracies of 2.6 fs, 1.39 ps^2, and 0.06 dB, respectively.

#123233 - $15.00 USD Received 25 Jan 2010; accepted 21 Feb 2010; published 16 Mar 2010

Table 4. Statistical results of 50 measurements

	Artifacts	Average	Maximum	Minimum	Max.–Min.
2-cm quartz DGD artifact (JME)	Average DGD in the wavelength range of 1530nm~1560nm with a λ step size of 2nm	627.02fs	627.033fs	627.000fs	0.033fs
	@1550nm with a λ step size of 2nm	627.757fs	627.955fs	627.567fs	0.388fs
2cm quartz DGD artifact (MMM)	Average DGD in the wavelength range of 1530nm~1560nm with a λ step size of 2nm	628.111fs	628.108fs	628.107fs	0.022fs
	@1550nm with a λ step size of 2nm	627.663fs	627.700s	627.511fs	0.189fs
SOPMD artifact (JME)	Average SOPMD in the range of 1550nm ~1552nm with a λ step size of 0.1nm	128.43 ps^2	129.64 ps^2	128.29 ps^2	1.35 ps^2
	SOPMD @ 1550nm with a λ step size of 0.1nm	129.31 ps^2	132.01 ps^2	126.70 ps^2	5.31 ps^2
SOPMD artifact (MMM)	Average SOPMD in the wavelength range of 1550nm~1552nm with a λ step size of 0.1nm	130.07ps^2	130.20 ps^2	129.92 ps^2	0.28 ps^2
	SOPMD @ 1550nm with a λ step size of 0.1nm	129.95 ps^2	131.40 ps^2	128.27 ps^2	3.13 ps^2
2-dB PDL artifact (JME)	Measured at 1550nm with different fiber pigtail positions	1.963	2.04dB	1.91dB	0.13dB
2-dB PDL artifact (MMM)	Measured at 1550nm with different fiber pigtail positions	1.965dB	1.982dB	1.941dB	0.041dB
0.4-dB PDL artifact (JME)	Measured at 1550nm with different fiber pigtail positions	0.389	0.437dB	0.326dB	0.11dB
0.4-dB PDL artifact (MMM)	Measured at 1550nm with different fiber pigtail positions	0.377dB	0.395dB	0.361dB	0.034 dB

5.5 PM fiber PER [37–39] and connector stress measurements

To minimize polarization dependent effects, it is often desirable to maintain a constant state of polarization as light propagates through an optical system. With regard to such systems, polarization extinction ratio (PER), or polarization crosstalk, is a measure of the degree to which the light is confined in the principal polarization mode. It is defined as the ratio of the power in the principal polarization mode to the power in the orthogonal polarization mode after propagation through the system, expressed in dB.

Polarization maintaining (PM) optical fibers have an optical (slow) axis defined by a strong linear birefringence. If light input to an ideal PM fiber is polarized along the fiber's optical axis, the state of polarization (SOP) will be maintained during propagation through the fiber. However, if the input light's SOP is misaligned, or the light is not fully polarized, the polarization component in the slow axis will propagate at a different speed from the polarization component aligned to the fast axis. Therefore, there will be a relative phase difference between the two polarization components. The resulting SOP at the exit of the fiber will change when the relative phase changes. For the case of a linearly polarized light beam

#123233 - $15.00 USD Received 25 Jan 2010; accepted 21 Feb 2010; published 16 Mar 2010

launched into a PM fiber with a misalignment angle of θ from the fiber's slow axis, as shown in Fig. 7, the extinction ratio due to the misalignment can be calculated as

$$PER = -10\log(\tan^2\theta) \tag{26}$$

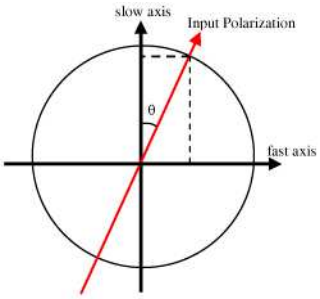

Fig. 7. A representation of linearly polarized light misaligned by an angle θ from the slow axis of a PM fiber

The PSA in the measurement system shown in Fig. 1 can be used to precisely measure the PER. If the slow axis of a PM fiber is aligned to the reference plane of the PSA at the PSA entrance, the normalized SOP can be calculated as

$$\begin{pmatrix} \cos 2\theta \\ \sin 2\theta\cos\delta \\ \sin 2\theta\sin\delta \end{pmatrix} \tag{27}$$

where θ and δ are the misalignment angle and the phase difference between the slow and fast axes, respectively. Variations in the input wavelength or in the fiber length due to temperature changes or mechanical stress will cause a variation in the relative phase δ, which in turn will cause the SOP to rotate about axis (1,0,0) on the Poincaré sphere when the relative phase δ is changed.

If the slow axis is misaligned to the PSA's reference plane by an angle 2ψ, the measured normalized polarization state can be expressed as:

$$\begin{pmatrix} \cos 2\psi\cos 2\theta - \sin 2\psi\sin 2\theta\cos\delta \\ \sin 2\psi\cos 2\theta + \cos 2\psi\sin 2\theta\cos\delta \\ \sin 2\theta\sin\delta \end{pmatrix} \tag{28}$$

It can be shown that the output SOP rotates about the slow axis (cos2ψ, sin2ψ, 0) to trace out a circle as δ increases or decreases, as illustrated in Fig. 8. Note that changes in wavelength, fiber length, or temperature will cause δ to change. The radius of the circle can be calculated to be R=sin2θ, and the PER can be calculated as

$$PER = -10\log\left(\frac{\sin^2\theta}{\cos^2\theta}\right) = -10\log\left(\frac{1-\cos 2\theta}{1+\cos 2\theta}\right) = -10\log\left(\frac{1-\sqrt{1-R^2}}{1+\sqrt{1-R^2}}\right) \tag{29}$$

#123233 - $15.00 USD Received 25 Jan 2010; accepted 21 Feb 2010; published 16 Mar 2010

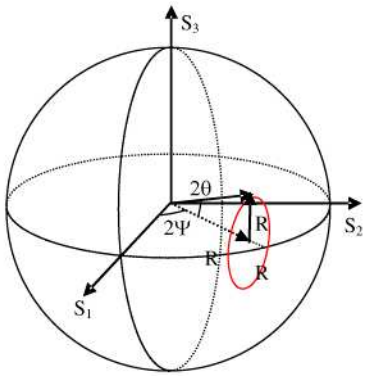

Fig. 8. Poincaré Sphere illustration of polarization state rotation of output light from a PM fiber due to wavelength variation or to thermal or mechanical stress

Essentially, the PER measured by our system, defined in Eq. (29), indicates the degree of linear polarization of light inside the PM fiber, or how well the input linear polarization is aligned with the slow (or fast) axis of the PM fiber. For a perfect polarization alignment, R approaches 0 (the circle collapses to a point), and the corresponding PER approaches infinity. At the other extreme, if the light power is equally split between the fast and slow axes, R approaches 1 (the SOP traces a great circle on the circumference of the Poincaré Sphere) and the corresponding PER approaches 0.

In our measurement system, because light output from the PM fiber is directly coupled into the PSA via free space, there is no alteration of the SOP before the light is analyzed. Consequently, the rotation axis of the circle is in the plane of the Poincaré sphere's equator and the angle Ψ is the angle between the slow axis and the reference plane of the PSA, as shown in Fig. 8. The PSA adapter has a reference key slot to accept a keyed PM fiber connector. Because the key slot is perpendicular to the PSA's reference plane, the angle between the slow axis of the PM fiber and the connector key is therefore 90-Ψ degrees. For example, Ψ=90° (the circle rotates around S_2 in Fig. 8) means that the slow axis of the PM fiber is vertical and aligned to the alignment key direction, and Ψ=0° indicates that the slow axis of the PM fiber is horizontal and perpendicular to the alignment key direction.

In practical measurement, the center of the circle generally deviates from the plane of the equator. This deviation is caused by stress induced birefringence and/or other polarization altering effects caused by the connector. The effect is equivalent to that of a PM fiber followed by a waveplate. Generally speaking, a greater deviation from the equator indicates a higher stress level. Such a measurement capability is very useful for PM fiber connectorization, because it can reveal information about whether an epoxy or a curing process used for the connectorization induces enough stress on the fiber to cause degradation of the polarization extinction ratio. The final degraded PER can be measured with a standard PER meter made with a rotating linear polarizer [37].

Figure 9 shows PER measurement results for two PM fibers with FC/PC connectors. The effect of stress is clearly shown in one of the PM connectors. In Fig. 9(A), the SOP evolution circle is centered on the equator, indicating negligible stress on the output fiber tip caused by connectorization. Consequently, the difference in PER values measured with our system and with a rotating polarizer is negligible. By contrast, in Fig. 9(B), the center of the SOP evolution circle is displaced from the equator, indicating a relatively large stress on the fiber. The stress induced birefringence of the output fiber tip can therefore be expected to degrade the output polarization extinction ratio. Indeed, the PER of the light after the output fiber connector is reduced to 31.1 dB measured with a rotating polarizer, although the PER of the light inside the fiber is as high as 39.6 dB measured with our measurement system.

In conclusion, by observing the size and position of the SOP evolution circle on the Poincaré Sphere, one can readily distinguish the PER degradation of a PM fiber caused by input SOP misalignment (size of the circle) from that caused by connectorization induced

#123233 - $15.00 USD Received 25 Jan 2010; accepted 21 Feb 2010; published 16 Mar 2010

stress (deviation of the circle from the equator). Such a capability is a useful tool for determining the quality of PM fiber connectorization by identifying stress induced birefringence.

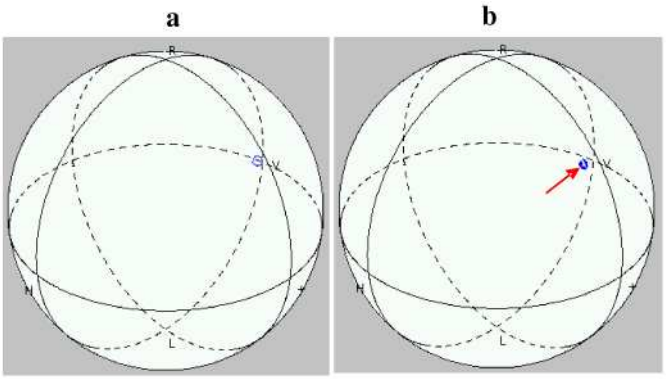

Fig. 9. PER measurement results: (A) PER measurement result with low stress on output FC/PC connector. (B) PER measurement result with relatively high stress on output FC/PC connector. The corresponding PER of light in the PM fiber is 39.6 dB; however, the PER of the output light is reduced to 31.1 dB due to stress induced birefringence. The deviation of the SOP evolution circle from the equator can be used to indicate stress induced birefringence at the exit end of the PM fiber.

5.6 PM fiber beat length estimation and results

Beat length is important because it measures how well a fiber maintains polarization. It is a measure of how fast the two orthogonal modes become decoupled and thus cease to exchange energy. Fibers with short beat lengths preserve polarization more strongly than those with long beat lengths.

Beat length L_B is defined by the ratio of the wavelength of the transmitted light λ to the fiber's phase birefringence Δn [40, 41],

$$L_B = \frac{\lambda}{\Delta n} \tag{30}$$

The beat length of PM fiber can be estimated by measuring its differential group delay (DGD) [40, 41]. The DGD measured by our measurement system is related to the group birefringence Δn_g by

$$DGD = \Delta n_g L / c \tag{31}$$

and the group birefringence is related to the phase birefringence by

$$\Delta n_g = \Delta n - \lambda \frac{d\Delta n}{d\lambda}. \tag{32}$$

The beat length can be calculated from the measured DGD by

$$L_B = \frac{\lambda}{\frac{DGD * c}{L} + \lambda \frac{d\Delta n}{d\lambda}} \tag{33}$$

If the chromatic dispersion equation of a fiber is

$$n^2 = 1 + \frac{B_1 \lambda^2}{\lambda^2 - C_1} + \frac{B_2 \lambda^2}{\lambda^2 - C_2} + \frac{B_3 \lambda^2}{\lambda^2 - C_3}, \tag{34}$$

#123233 - $15.00 USD Received 25 Jan 2010; accepted 21 Feb 2010; published 16 Mar 2010

the beat length can be calculated from

$$L_B = \frac{\lambda * y}{\frac{DGD * c}{L}} \tag{35}$$

where

$$y = 1 - \frac{1}{n}\left[n^2 - 1 - \left(\frac{B_1\lambda^4}{(\lambda^2 - C_1)^2} + \frac{B_2\lambda^4}{(\lambda^2 - C_2)^2} + \frac{B_3\lambda^4}{(\lambda^2 - C_3)^2}\right)\right] \tag{36}$$

We measured the beat length of a 1.16m Panda PM fiber and obtained a DGD of 1.578ps. The corresponding beat length from Eq. (36) is 3.86mm, consistent with the manufacturer's specified value of 3~5mm [42].

For a PM fiber with $DGD_{\lambda 2} \approx DGD_{\lambda 1}$, the beat length at λ_2 can be estimated by using the beat length measurement result at λ_1:

$$L_{B\lambda_2} = \frac{\lambda_2}{\lambda_1} L_{B\lambda_1} \tag{37}$$

For example, if we measure the DGD and beat length L_{B1550} of a PM fiber at 1550 nm, its beat length L_{B1310} at 1310 nm is simply $L_{B1310}=(1310/1550)L_{B1550}=0.845L_{B1550}$.

6 Summary

In summary, we describe a novel polarization measurement system consisting of a binary MO polarization state generator (PSG), a binary MO polarization state analyzer, a tunable laser, and a personal computer. Because of its binary nature, the system can be easily calibrated against imperfections in the optical components used in the system, caused by wavelength and environmental variations. Consequently, we have achieved the unprecedented PMD measurement sensitivity or resolution of 1 fs, PMD measurement accuracy of 2.6 fs, PMD measurement repeatability of 0.022 fs, SOPMD resolution of 0.005 ps^2, SOPMD accuracy of 1.39 ps^2, SOPMD repeatability of 0.28 ps^2, PDL resolution of 0.01 dB, PDL accuracy of 0.06 dB, and PDL repeatability of 0.034 dB. We also describe and demonstrate some other interesting applications of the system, including PER measurement, PM fiber connector stress analysis, and PM fiber beat length measurement. This extremely accurate polarization measurement system will find a wide range of applications in optical component characterization, optical fiber link characterization, PM fiber connectorization, and PM fiber characterization.

Acknowledgements

We thank Lynn Lin, Heming Zhang, and Qing Wan of General Photonics Corporation for mechanical, electronics and software designs used in this paper. We also thank Susan Wey for the proof-reading of the manuscript. This work was supported by a research funding of General Photonics Corporation.